

On the stability of a growing annular hyperelastic plate

Sumit Mehta¹, Gangadharan Raju¹, Prashant Saxena^{*2}

¹*Department of Mechanical and Aerospace Engineering
Indian Institute of Technology Hyderabad, India*

²*James Watt School of Engineering, University of Glasgow, Glasgow G12 8LT, UK*

Abstract

Growth-induced instabilities are ubiquitous in biological systems and lead to diverse morphologies in the form of wrinkling, folding, and creasing. The current work focusses on the mechanics behind growth-induced wrinkling instabilities in an incompressible annular hyperelastic plate subjected to two types of boundary constraints. Governing differential equations for a two-dimensional plate system are derived using a variational principle and series expansion along the thickness direction. The incremental differential equations for studying the bifurcation behaviour of the growing hyperelastic annular plate are derived by considering both axisymmetric and asymmetric perturbations. The resulting equations are then solved numerically using the compound matrix method to evaluate the critical growth stretch that causes bifurcation. The effect of boundary constraints, thickness, and radius ratio of the annular plate on the critical growth factor is studied. For most of the considered cases, an asymmetric bifurcation is the preferred mode of instability for an annular plate. The obtained results are relevant to modelling of wrinkling phenomena in planar soft tissues, pattern transition in two-dimensional films growing on an elastic substrate, and manufacturing of smart materials.

Keywords: Growth, plate theory, bifurcation, finite elasticity

1 Introduction

Growth process typically involves change of body mass and generation of residual stresses in an evolving system which induces large deformation that triggers the mechanical instabilities. These growth-induced instabilities lead to formation of diverse patterns in the form of wrinkling, folding, creasing (Li et al., 2012) that are critical to biological systems such as plants (Dai and Liu, 2014; Coen et al., 2004), tissues, and organs (Ambrosi et al., 2011). Moreover, certain anomalies in human biological systems like narrowing airways due to asthma (Wiggs et al., 1997), and malformation of cerebral cortex (Raybaud and Widjaja, 2011) give rise to patterns which defines a new physiological function of the biological system. Irregular wrinkles generated during cutaneous wound healing are studied to avoid scar formation (Cerda, 2005; Nassar et al., 2012). Besides biological applications, pattern formation and their transition during growth (remodelling) have been extensively studied from a purely mechanics aspect (Ben Amar and Goriely, 2005; Cao et al., 2012; Budday et al., 2014; Balbi and Ciarletta, 2013; Limbert and Kuhl, 2018). Instabilities in soft solids such as swollen hydrogels (Ionov, 2013) and elastomers (Kempaiah and Nie, 2014) are useful to create desired patterns which have been utilised in the

*Corresponding author email: prashant.saxena@glasgow.ac.uk

design of stretchable electronics (Khang et al., 2009), smart morphable surfaces in aerodynamics control (Terwagne et al., 2014), wearable communication devices (Rogers et al., 2010), and shape-shifting structures (Stein-Montalvo et al., 2019). Therefore, it is fundamentally important to understand the mechanics of growth which regulates the instabilities in soft growing bodies. To accomplish this, a consistent mathematical model is necessary and the continuum mechanics approach provides the appropriate framework for growth-induced instabilities in morphing structures (Kuhl, 2014; Goriely, 2017).

To describe the kinematics of growth, the total deformation gradient is decomposed to a growth tensor and an elastic deformation tensor (Rodriguez et al., 1994). The former tensor describes the local change in volume with addition/subtraction of material, can be incompatible due to non-uniform growth in the neighbourhood of a material point (Garikipati et al., 2004; Goriely and Ben Amar, 2007). In order to ensure the compatibility and integrity of the total deformation, the elastic deformation tensor is required. This generally results in residual stresses that can trigger mechanical instabilities. Based on this theory, growth-induced instabilities in soft biological tissues are extensively studied (Ben Amar and Goriely, 2005; Li et al., 2012; Wu and Ben Amar, 2015; Liu et al., 2020b, 2021).

In many existing works, a hyperelastic membrane model is used to study instabilities in thin soft tissues (Papastavrou et al., 2013; Swain and Gupta, 2015, 2016). The interplay between growth and elasticity induces large deformation and one needs to adopt consistent plate or shell theories to capture the combined effect of bending and stretching deformation simultaneously. Classical plate theories like Kirchhoff-Love, Föppl-von Kármán and Mindlin-Reisner theory have been widely used to investigate the bifurcation behaviour of thin elastic structures (Coman and Haughton, 2006; Coman et al., 2015; Li et al., 2010), and liquid crystal elastomers (Mihai and Goriely, 2020). Dervaux et al. (2009) derived the Föppl-von Kármán plate theory and Goriely and Ben Amar (2005) used the elastic shell theory to investigate growth-induced patterns. However, these theories are suitable for small strain problems and also based on apriori assumptions of displacement variation along thickness of the plate. As a result, they give inconsistent results when applied to finite strain problems and general loading conditions. To overcome the limitations of classical plate theories, Kienzler (2002) proposed a consistent asymptotic plate theory based on linear elasticity which does not apply any kinematic assumptions and all the unknowns are treated as independent variables. Dai and Song (2014) proposed a finite strain plate theory for compressible hyperelastic material based on the principle of minimisation of potential energy under three-dimensional loading conditions. Wang et al. (2016) extended this approach to incompressible hyperelastic materials with additional Lagrange multiplier to accommodate the incompressibility constraint. Wang et al. (2018) derived a consistent finite-strain plate theory for growth-induced large deformation and investigated the buckling and post-buckling behaviour of a thin rectangular hyperelastic plate under axial growth. Recently, the finite strain asymptotic plate theory has been applied to study the plane strain problems of growth-induced deformation in single and multi-layered hyperelastic plates (Wang et al., 2019b; Du et al., 2020). Liu et al. (2020a) discussed the large elastic deformation in nematic liquid crystal elastomer and the authors of the present paper (Mehta et al., 2021b) investigated the bifurcation behaviour of circular hyperelastic plate under the influence of growth using finite strain asymptotic plate theory. To understand the characteristics of growth-induced instabilities in biological systems, the bifurcation behaviour needs to be investigated (Vandiver and Goriely, 2009). The governing system of equations for performing bifurcation analysis are complicated and involve nonlinear partial differential equations (PDEs) which can be solved using various numerical approaches (Dortdivanlioglu et al., 2017; Kadapa et al., 2021).

The current work investigates wrinkling phenomena in growing hyperelastic annular plate that can be naturally observed in human tissues and plants (Liang and Mahadevan, 2009; Steele, 2000) when subjected to different boundary constraints as shown in Figure 1. For example, in a circular shaped leaf, the inner part is normally stiffer (approximated by a clamped boundary condition) than the outer part

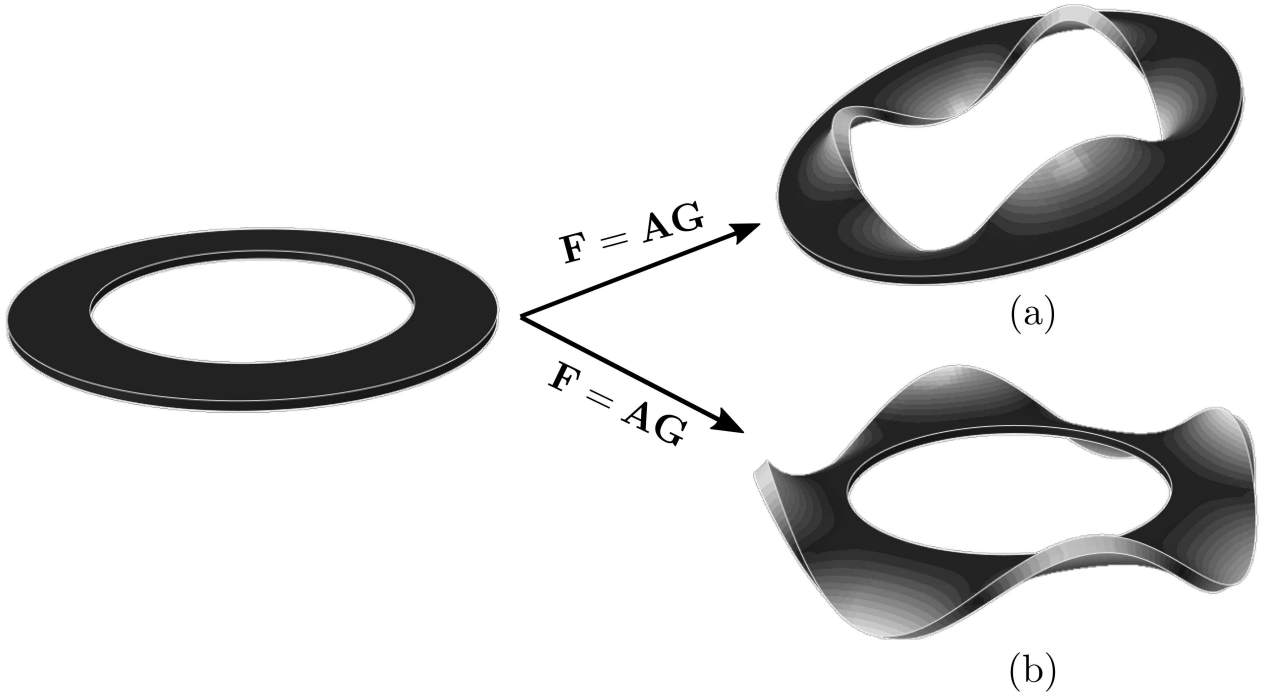


Figure 1: Possible out-of-plane wrinkled configurations of a hyperelastic annular plate growing with in-plane growth function when subjected to different type of boundary conditions i.e., (a) constrained outer boundary and unconstrained inner boundary, and (b) constrained inner boundary and unconstrained outer boundary. In each case, the unconstrained boundary exhibit wrinkles in circumferential direction induced by growth.

and the growth induces wrinkling patterns at the outer edge of the leaf (Liu et al., 2013) similar to Figure 1b. To understand the mechanics of growth in annular plate structures, we assume externally-driven homogeneous isotropic growth. The growth function is considered as a control parameter responsible for the change of shape (Wang et al., 2019b; Li et al., 2022) and onset of instability. We have applied the consistent finite strain plate theory introduced by Wang et al. (2018) to derive the governing differential equations (GDEs) for general loading conditions. A plane-stress assumption along with a neo-Hookean material model is employed to simplify these equations. Subsequently, we perform the stability analysis by perturbing the principal solution subjected to two different cases of boundary condition. In the first case, the inner boundary of the annular plate is unconstrained and the outer boundary is constrained. For the second case, the inner boundary of the plate is constrained and outer boundary is unconstrained. The resulting nonlinear ordinary differential equations (ODEs) are solved numerically to evaluate the critical value of growth parameter. For each case of boundary conditions, we investigate the type of perturbation namely, axisymmetric or asymmetric which minimises the bifurcation solution of the annular plate and also study the effect of plate thickness, radius ratio on the onset of instability.

1.1 Organisation of this manuscript

The remainder of this paper is organised as follows. In Section 2, a general formulation for three-dimensional annular plate is established and then the same is reduced to a two-dimensional system by eliminating the dependence of thickness variable using series approximation. In Section 3, we discuss the principal solution associated with the growth-induced deformation in an incompressible neo-Hookean annular plate subjected to two different boundary conditions. In Section 4, we derive the non-dimensional nonlinear ODEs associated with asymmetric as well as axisymmetric perturbations.

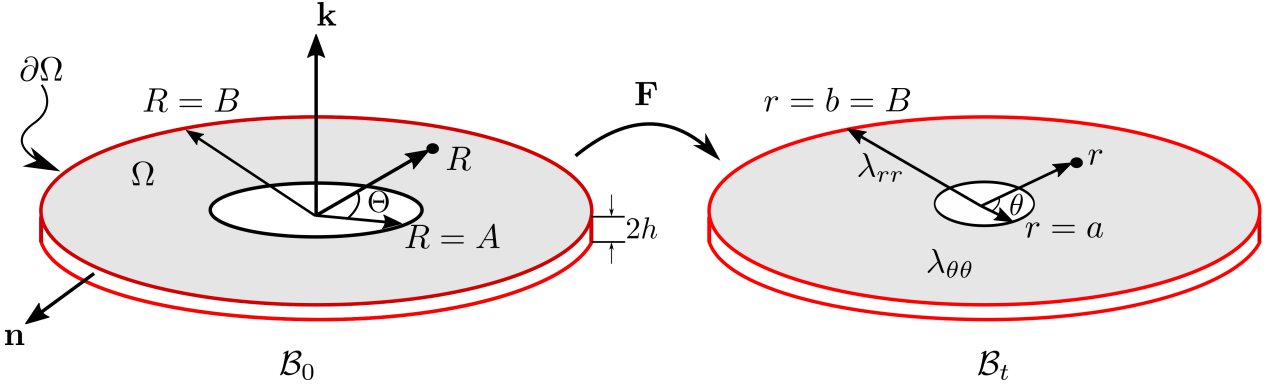


Figure 2: A schematic of finite deformation of an annular plate due to growing region Ω with constrained outer boundary. The region Ω is growing with a factor of λ_{rr} and $\lambda_{\theta\theta}$ in the radial and hoop directions, respectively.

Then, in Section 5, we apply compound matrix method to solve the bifurcation problem and compare the bifurcation solutions associated with each type of perturbation and boundary conditions. Finally, we conclude the work in Section 6. Supplementary mathematical derivations are provided in the Appendix.

1.2 Notation

Brackets: Two types of brackets are used. Round brackets () are used to define the functions applied on parameters or variables. Square brackets [] are used to clarify the order of operations in an algebraic expression. Square brackets are also used for matrices and tensors. At some places we use the square bracket to define the functional.

Symbols: A variable typeset in a normal weight font represents a scalar. A lower-case bold weight font denotes a vector and bold weight upper-case denotes tensor or matrices. Tensor product of two vectors \mathbf{a} and \mathbf{b} is defined as $[\mathbf{a} \otimes \mathbf{b}]_{ij} = [\mathbf{a}]_i [\mathbf{b}]_j$. Tensor product of two second order tensors \mathbf{A} and \mathbf{B} is defined as either $[\mathbf{A} \otimes \mathbf{B}]_{ijkl} = [\mathbf{A}]_{ij} [\mathbf{B}]_{kl}$ or $[\mathbf{A} \boxtimes \mathbf{B}]_{ijkl} = [\mathbf{A}]_{ik} [\mathbf{B}]_{jl}$. Higher order tensors are written in bold calligraphic font with a superscript as $\mathcal{A}^{(i)}$, where superscript ‘ i ’ tells that the function is differentiated $i+1$ times. For example, $\mathcal{A}^{(1)} = \frac{\partial f(\mathbf{A})}{\partial \mathbf{A} \partial \mathbf{A}}$ is a fourth order tensor. Operation of a fourth order tensor on a second order tensor is denoted as $[\mathcal{A}^{(1)} : \mathbf{A}]_{ij} = [\mathcal{A}^{(1)}]_{ijkl} [\mathbf{A}]_{kl}$. Inner product is defined as $\mathbf{a} \cdot \mathbf{b} = [\mathbf{a}]_i [\mathbf{b}]_i$ and $\mathbf{A} : \mathbf{B} = [\mathbf{A}]_{ij} [\mathbf{B}]_{ij}$. The symbol ∇ denotes the two-dimensional differentiation operator. We use the word ‘Div’ to denote divergence in three dimensions.

Functions: $\det(\mathbf{A})$ denote the determinant of the tensor \mathbf{A} . $\text{tr}(\mathbf{A})$ denote the trace of a tensor \mathbf{A} . $\text{diag}(a, b, c)$ denotes a second order tensor with only diagonal entries a, b and c .

2 Governing equation with variational principle

Consider a thin annular plate with constant thickness ($2h$) occupying the region $\Omega \times [0, 2h]$ in the reference configuration $\mathcal{B}_0 \in \mathcal{R}^3$ and then deforms to the current configuration $\mathcal{B}_t \in \mathcal{R}^3$ as shown in Figure 2. Coordinates of a point in the undeformed configuration are given by R, Θ, Z and in the deformed configuration by r, θ, z . Position vector in \mathcal{B}_0 is denoted as $\mathbf{X}(R, \Theta, Z)$ and denoted as $\mathbf{x}(r, \theta, z)$ in \mathcal{B}_t . The inner and outer radii in the reference configuration are denoted as A and B , and the same in deformed configuration are denoted as a and b , respectively (see Figure 2). Using the position vector \mathbf{X} and \mathbf{x} , the deformation gradient is expressed as $\mathbf{F} = \frac{\partial \mathbf{x}}{\partial \zeta} + \frac{\partial \mathbf{x}}{\partial Z} \otimes \mathbf{k}$, where $\zeta = R\mathbf{e}_R + \Theta\mathbf{e}_\Theta$ and \mathbf{k} is the

unit normal to the surface Ω in the reference configuration. Following the multiplicative decomposition approach proposed by Rodriguez et al. (1994), the total deformation gradient of a growing plate is defined as $\mathbf{F} = \mathbf{AG}$ in $A \leq R \leq B$, where \mathbf{G} represents the growth tensor and \mathbf{A} represents the elastic deformation tensor. We also assume the material to be incompressible and therefore to follow the constraint $L(\mathbf{F}, \mathbf{G}) = L_0(\mathbf{FG}^{-1}) = \det(\mathbf{A}) - 1 = 0$. The energy density (ϕ) per unit volume of the material is assumed as $\phi(\mathbf{F}, \mathbf{G}) = J_G \phi_0(\mathbf{FG}^{-1})$, where $J_G = \det(\mathbf{G}) = \det(\mathbf{F})$ describes the local change in volume due to growth and $\phi_0(\mathbf{FG}^{-1})$ is the elastic strain energy density. If we neglect the body force, the total potential energy functional (ψ) for the incompressible plate is

$$\psi[\mathbf{x}(\mathbf{X}), p(\mathbf{X})] = \int_{\Omega} \int_0^{2h} J_G \phi_0(\mathbf{FG}^{-1}) dV - \int_{\Omega_1} \int_0^{2h} [J_G p(\mathbf{X}) L_0(\mathbf{FG}^{-1})] dV, \quad (2.1)$$

where $p(\mathbf{X})$ is the Lagrange multiplier associated with the incompressibility constraint. We apply the principle of minimum potential energy and vanishing of the first variation with respect to \mathbf{x} and p of the above functional results in the GDEs with traction free boundary conditions

$$\text{Div } \mathbf{P} = \mathbf{0}, \quad \text{in } \Omega \times [0, 2h], \quad (2.2a)$$

$$\mathbf{Pk}|_{Z=0} = \mathbf{0}, \quad \mathbf{Pk}|_{Z=2h} = \mathbf{0}, \quad \text{on } \Omega, \quad (2.2b)$$

$$\mathbf{Pn}|_{R=A} = \mathbf{0}, \quad \mathbf{Pn}|_{R=B} = \mathbf{0}, \quad \text{on } \partial\Gamma \times [0, 2h], \quad (2.2c)$$

and the incompressibility constraint, i.e., $\det(\mathbf{A}) - 1 = 0$. Here, \mathbf{n} is the unit outward normal to the lateral boundary ($\partial\Gamma$) and $\mathbf{P} = J_G \left[\frac{\partial \phi_0}{\partial \mathbf{A}} - p \frac{\partial L_0}{\partial \mathbf{A}} \right] \mathbf{G}^{-T}$ in Ω is recognised as the first Piola Kirchhoff stress tensor.

2.1 2-D plate model

To obtain the 2-D formulation for the annular plate, we apply a series expansion of the unknown variables, \mathbf{x} and p about the bottom surface of plate ($Z = 0$) along the thickness direction given by

$$\mathbf{x}(\mathbf{X}) = \sum_{n=0}^3 \frac{Z^n}{n!} \mathbf{x}^{(n)}(\zeta) + O(Z^4), \quad \text{and} \quad p(\mathbf{X}) = \sum_{n=0}^3 \frac{Z^n}{n!} p^{(n)}(\zeta) + O(Z^4), \quad (2.3)$$

where we have used the notation $\mathbf{x}^{(n)} = \frac{\partial^n \mathbf{x}}{\partial Z^n}$ and $p^{(n)} = \frac{\partial^n p}{\partial Z^n}$. Using (2.3), we obtain the recursion relation for deformation gradient as, $\mathbf{F}^{(n)} = \nabla \mathbf{x}^{(n)} + \mathbf{x}^{(n+1)} \otimes \mathbf{k}$. Similarly, we expand the elastic tensor \mathbf{A} , and inverse transpose of growth tensor (\mathbf{G}^{-T}) to obtain the Piola Kirchhoff stress tensor \mathbf{P} (see Appendix A). Upon neglecting the body force and external traction, the stress equilibrium equation (2.2a) is given as the recursion relation

$$\nabla \cdot \mathbf{P}^{(n)} + \mathbf{P}^{(n+1)} \mathbf{k} = \mathbf{0}, \quad \text{for } n = 0, 1, 2. \quad (2.4)$$

Substituting $\mathbf{A} = \mathbf{FG}^{-1}$ in the expression of Piola stress obtained as $\mathbf{P} = J_G \left[\frac{\partial \phi_0}{\partial \mathbf{A}} - p \frac{\partial L_0}{\partial \mathbf{A}} \right] \mathbf{G}^{-T}$ and making use of (2.4), we obtain the explicit expressions of $\mathbf{P}^{(0)}$, $\mathbf{P}^{(1)}$, and $\mathbf{P}^{(2)}$ which in component form ($[\mathbf{P}]_{ij} = P_{ij}$) are given as

$$P_{ij}^{(0)} = J_G \left[\mathbf{A}^{(0)} - p^{(0)} \mathbf{L}^{(0)} \right]_{i\alpha} \bar{G}_{\alpha j}^{(0)}, \quad (2.5a)$$

$$P_{ij}^{(1)} = J_G \left[\left[[\mathbf{A}^{(1)} - p^{(0)} \mathbf{L}^{(1)}]_{i\alpha k\beta} A_{k\beta}^{(1)} - p^{(1)} \mathbf{L}_{i\alpha}^{(0)} \right] \bar{G}_{\alpha j}^{(0)} + [\mathbf{A}^{(0)} - p^{(0)} \mathbf{L}^{(0)}]_{i\alpha} \bar{G}_{\alpha j}^{(1)} \right], \quad (2.5b)$$

$$P_{ij}^{(2)} = J_G \left[\left[\mathcal{A}_{ik\alpha\beta}^{(1)} A_{\alpha\beta}^{(2)} + [\mathbf{A}^{(2)} - p^{(0)} \mathbf{L}^{(2)}]_{ik\alpha\beta mn} A_{\alpha\beta}^{(1)} A_{mn}^{(1)} - 2p^{(1)} \mathbf{L}_{ik\alpha\beta}^{(1)} A_{\alpha\beta}^{(1)} - p^{(0)} \mathbf{L}_{ik\alpha\beta}^{(1)} A_{\alpha\beta}^{(2)} \right. \right. \\ \left. \left. - p^{(2)} \mathbf{L}_{ik}^{(0)} \right] \bar{G}_{kj}^{(0)} + \left[2\mathcal{A}_{ik\alpha\beta}^{(1)} A_{\alpha\beta}^{(1)} - 2p^{(0)} \mathbf{L}_{ik\alpha\beta}^{(1)} A_{\alpha\beta}^{(1)} - 2p^{(1)} \mathbf{L}_{ik}^{(0)} \right] \bar{G}_{kj}^{(1)} + \left[\mathbf{A}^{(0)} - p^{(0)} \mathbf{L}^{(0)} \right]_{ik} \bar{G}_{kj}^{(2)} \right], \quad (2.5c)$$

with $\mathbf{A}^{(i)}(\mathbf{A}^{(0)}) = \frac{\partial^{i+1} \phi_0(\mathbf{A})}{\partial \mathbf{A}^{i+1}} \Big|_{\mathbf{A}=\mathbf{A}^{(0)}}$ and $\mathbf{L}^{(i)}(\mathbf{A}^{(0)}) = \frac{\partial L_0(\mathbf{A})}{\partial \mathbf{A}^{i+1}} \Big|_{\mathbf{A}=\mathbf{A}^{(0)}}$. Further mathematical details of the above calculations are provided in the supplementary document. Equations (2.5b) – (2.5c) involve higher derivatives of \mathbf{A} which are obtained using the series expansion of \mathbf{F} and \mathbf{G}^{-T}

$$\mathbf{A}^{(0)} = \mathbf{F}^{(0)} \bar{\mathbf{G}}^{(0)T}, \quad \mathbf{A}^{(1)} = \mathbf{F}^{(0)} \bar{\mathbf{G}}^{(1)T} + \mathbf{F}^{(1)} \bar{\mathbf{G}}^{(0)T}, \quad \mathbf{A}^{(2)} = \mathbf{F}^{(0)} \bar{\mathbf{G}}^{(2)T} + 2\mathbf{F}^{(1)} \bar{\mathbf{G}}^{(1)T} + \mathbf{F}^{(2)} \bar{\mathbf{G}}^{(0)T}. \quad (2.6)$$

The stress free boundary conditions on the bottom and top surfaces of the annular plate are obtained from equations (2.2a) – (2.2c) as

$$\mathbf{P}\mathbf{k}|_{Z=0} = \mathbf{P}^{(0)}(\mathbf{A})\mathbf{k} = \mathbf{0}, \quad (2.7a)$$

$$\mathbf{P}\mathbf{k}|_{Z=2h} = \mathbf{P}^{(0)}\mathbf{k} + 2h\mathbf{P}^{(1)}\mathbf{k} + 2h^2\mathbf{P}^{(2)}\mathbf{k} + O(h^3) = \mathbf{0}, \quad (2.7b)$$

and the conditions associated with the incompressibility constraint are given by

$$L_0(\mathbf{A}^{(0)}) = 0, \quad \mathbf{L}^{(0)}[\mathbf{A}^{(1)}] = 0, \quad \mathbf{L}^{(0)}[\mathbf{A}^{(2)}] + \mathbf{L}^{(1)}[\mathbf{A}^{(1)}, \mathbf{A}^{(1)}] = 0, \quad (2.8) \\ \mathbf{L}^{(0)}[\mathbf{A}^{(3)}] + 3\mathbf{L}^{(1)}[\mathbf{A}^{(1)}, \mathbf{A}^{(2)}] + \mathbf{L}^{(2)}[\mathbf{A}^{(1)}, \mathbf{A}^{(1)}, \mathbf{A}^{(1)}] = 0,$$

where $\mathbf{L}^{(0)}[\mathbf{A}^{(1)}] = \mathbf{L}^{(0)} : \mathbf{A}^{(1)} = \det(\mathbf{A})\mathbf{A}^{-T} : \mathbf{A}^{(1)}$. On subtracting the top (2.7b) and bottom (2.7a) traction conditions we obtain the 2-D plate GDE

$$\nabla \cdot \tilde{\mathbf{P}} = \mathbf{0}. \quad (2.9)$$

Here, $\tilde{\mathbf{P}} = \mathbf{P}^{(0)} + h\mathbf{P}^{(1)} + \frac{2}{3}h^2\mathbf{P}^{(2)}$ is the average stress obtained by simply taking the integration over the thickness of the plate, $\tilde{\mathbf{P}} = \frac{1}{2h} \int_0^{2h} \mathbf{P} dZ$. Using the series expansion approach, the equilibrium equation (2.9) is expressed as

$$\left. \begin{aligned} \nabla \cdot \mathbf{P}_t^{(0)} + h\nabla \cdot \mathbf{P}_t^{(1)} + \frac{2}{3}h^2 \nabla \cdot \mathbf{P}_t^{(2)} + O(h^3) &= \mathbf{0}, \\ [\nabla \cdot \tilde{\mathbf{P}}] \cdot \mathbf{k} = \nabla \cdot [\mathbf{P}^{(0)T} \mathbf{k}] + h\nabla \cdot [\mathbf{P}^{(1)T} \mathbf{k}] + \frac{2}{3}h^2 \nabla \cdot [\mathbf{P}^{(2)T} \mathbf{k}] + O(h^3) &= \mathbf{0}, \end{aligned} \right\} \quad (2.10)$$

where the subscript ‘*t*’ represents the in-plane (or tangential) component of a vector or tensor. Equation (2.10) is then reduced to a refined plate equation (Wang et al., 2019a; Yu et al., 2020) by neglecting the contribution of $\mathbf{P}^{(2)}$ but keeping the terms of $O(h^2)$ that correspond to the bending energy of the plate

$$\nabla \cdot \mathbf{P}_t^{(0)} + h\nabla \cdot \mathbf{P}_t^{(1)} = \mathbf{0}, \quad (2.11a)$$

$$\nabla \cdot [(\mathbf{P}^{(0)T} \mathbf{k}) - (\mathbf{P}^{(0)} \mathbf{k})] + h \left[\nabla \cdot [(\mathbf{P}^{(1)T} \mathbf{k}) - (\mathbf{P}^{(1)} \mathbf{k})] \right] + \frac{1}{3}h^2 \nabla \cdot [\nabla \cdot \mathbf{P}_t^{(1)}] = 0, \quad (2.11b)$$

The explicit expressions of unknowns variables $\mathbf{x}^{(2)}$, $p^{(1)}$ and $\mathbf{x}^{(3)}$, $p^{(2)}$ in terms of $\mathbf{x}^{(0)}$, $\mathbf{x}^{(1)}$ and $p^{(0)}$ which result in a closed form system are provided in our previous work (Mehta et al., 2021b).

3 Growth induced deformation

In this section, we discuss the deformation of an annular plate undergoing isotropic growth i.e., plate growing with equivalent constant growth factor (λ) in the radial and circumferential directions. The growth tensor \mathbf{G} then takes the form $\text{diag}(\lambda_{rr}, \lambda_{\theta\theta}, 1)$ where $\lambda_{rr} = \lambda_{\theta\theta} = \lambda$. The plate is assumed to be made up of an incompressible neo-Hookean material with elastic strain-energy function $\phi(\mathbf{F}, \mathbf{G}) = J_G \phi_0(\mathbf{A}) = J_G C_0 [I_1 - 3]$, where $I_1 = \text{tr}(\mathbf{A}^T \mathbf{A})$ and $2C_0$ is the ground state shear modulus. Using (2.3), the series approximation of unknown variables about the bottom surface in the cylindrical coordinate system is given as

$$\begin{aligned} r(R, Z) &= \sum_{n=0}^{n=3} \frac{Z^n}{n!} r^{(n)}(R) + O(Z^4), & \theta(R, Z) &= \sum_{n=0}^{n=3} \frac{Z^n}{n!} \theta^{(n)}(R) + O(Z^4), \\ z(R, Z) &= \sum_{n=0}^{n=3} \frac{Z^n}{n!} z^{(n)}(R) + O(Z^4), & p(R, Z) &= \sum_{n=0}^{n=3} \frac{Z^n}{n!} p^{(n)}(R) + O(Z^4), \end{aligned} \quad (3.1)$$

where $(\cdot)^n = \frac{\partial^n(\cdot)}{\partial Z^n}$. The isotropic growth field with (3.1) results in

$$[\bar{\mathbf{G}}^{(0)}] = \begin{bmatrix} \frac{1}{\lambda} & 0 & 0 \\ 0 & \frac{1}{\lambda} & 0 \\ 0 & 0 & 1 \end{bmatrix}, \quad [\mathbf{F}^{(0)}] = \begin{bmatrix} \frac{\partial r^{(0)}}{\partial R} & \frac{1}{R} \frac{\partial r^{(0)}}{\partial \Theta} & r^{(1)} \\ r^{(0)} \frac{\partial \theta^{(0)}}{\partial R} & \frac{r^{(0)} \partial \theta^{(0)}}{R} & r^{(0)} \theta^{(1)} \\ \frac{\partial z^{(0)}}{\partial R} & \frac{1}{R} \frac{\partial z^{(0)}}{\partial \Theta} & z^{(1)} \end{bmatrix}, \quad J_G = \det(\mathbf{G}) = \lambda^2, \quad (3.2)$$

where $\bar{\mathbf{G}}^{(0)}$ and $\mathbf{F}^{(0)}$ are the first terms in the expansion of \mathbf{G}^{-T} and \mathbf{F} , respectively. Explicit expressions for the unknown variables can be derived as

$$p^{(0)} = \frac{2C_0\lambda^4}{|\nabla \mathbf{x}^{(0)*}|^2}, \quad r^{(1)} = \frac{p^{(0)}\Delta x_{11}}{2C_0\lambda^2}, \quad \theta^{(1)} = \frac{p^{(0)}\Delta x_{22}}{2C_0\lambda^2 r^{(0)}}, \quad z^{(1)} = \frac{p^{(0)}\Delta x_{33}}{2C_0\lambda^2}. \quad (3.3)$$

Equations associated with the derivation of (3.3) and the terms corresponding to higher orders of $\bar{\mathbf{G}}$, \mathbf{F} are detailed in Appendix A.

3.1 Pre-buckling solution

The principal or pre-buckling axisymmetric solution is given by

$$r^{(0)}(R) = r(R), \quad \theta^{(0)} = \Theta, \quad z^{(0)}(R) = C_Z, \quad (3.4)$$

where C_Z is a constant function. Upon substituting the principal solution (3.4) in the plate equation (2.11), we obtain a fourth order equation in $r^{(0)}$. This is transformed to four first order ODEs of the form

$$\mathbf{D}\mathbf{y}' = \mathbf{q}, \quad (3.5)$$

where a prime denotes derivative with respect to R , $\mathbf{D} = \text{diag}(1, 1, 1, \mathcal{D}_1)$, $\mathbf{y}' = [y'_1 \ y'_2 \ y'_3 \ y'_4]^T$, $\mathbf{q} = [y_2 \ y_3 \ y_4 \ \mathcal{D}_2]^T$, and \mathcal{D}_1 and \mathcal{D}_2 are given as

$$\mathcal{D}_1 = 2\rho_1^3 \rho_2^2 \rho^6 \bar{h}^2 \lambda^6 \left[4\rho^2 \lambda^6 + \rho_1^2 \rho_2^4 \right],$$

$$\begin{aligned}
\mathcal{D}_2 = & 80 \bar{h}^2 \lambda^{12} \rho^8 \rho_1^3 \rho_2 \rho_3 \rho_4 - 72 \bar{h}^2 \lambda^{12} \rho^8 \rho_1^3 \rho_3^3 + 24 \bar{h}^2 \lambda^{12} \rho^8 \rho_1^2 \rho_2^3 \rho_4 + 64 \bar{h}^2 \lambda^{12} \rho^8 \rho_1^2 \rho_2^2 \rho_3^2 \\
& + 82 \bar{h}^2 \lambda^{12} \rho^8 \rho_1 \rho_2^4 \rho_3 - 6 \bar{h}^2 \lambda^{12} \rho^8 \rho_2^6 - 32 \bar{h}^2 \lambda^{12} \rho^7 \rho_1^3 \rho_2^2 \rho_4 - 24 \bar{h}^2 \lambda^{12} \rho^7 \rho_1^3 \rho_2 \rho_3^2 \\
& - 200 \bar{h}^2 \lambda^{12} \rho^7 \rho_1^2 \rho_2^3 \rho_3 - 82 \bar{h}^2 \lambda^{12} \rho^7 \rho_1 \rho_2^5 + 144 \bar{h}^2 \lambda^{12} \rho^6 \rho_1^3 \rho_2^2 \rho_3 + 136 \bar{h}^2 \lambda^{12} \rho^6 \rho_1^2 \rho_2^4 \\
& - 24 \bar{h}^2 \lambda^6 \rho^6 \rho_1^5 \rho_2^5 \rho_3 \rho_4 + 80 \bar{h}^2 \lambda^6 \rho^6 \rho_1^5 \rho_2^4 \rho_3^3 - 8 \bar{h}^2 \lambda^6 \rho^6 \rho_1^4 \rho_2^7 \rho_4 + 86 \bar{h}^2 \lambda^6 \rho^6 \rho_1^4 \rho_2^6 \rho_3^2 \\
& + 57 \bar{h}^2 \lambda^6 \rho^6 \rho_1^3 \rho_2^8 \rho_3 + 20 \bar{h}^2 \lambda^6 \rho^6 \rho_1^2 \rho_2^{10} + 9 \lambda^8 \rho^6 \rho_1^5 \rho_2^6 \rho_3 + 9 \lambda^8 \rho^6 \rho_1^4 \rho_2^8 - 48 \bar{h}^2 \lambda^{12} \rho^5 \rho_1^3 \rho_2^3 \\
& - 4 \bar{h}^2 \lambda^6 \rho^5 \rho_1^5 \rho_2^6 \rho_4 - 56 \bar{h}^2 \lambda^6 \rho^5 \rho_1^5 \rho_2^5 \rho_3^2 - 36 \bar{h}^2 \lambda^6 \rho^5 \rho_1^4 \rho_2^7 \rho_3 + 9 \bar{h}^2 \lambda^6 \rho^5 \rho_1^3 \rho_2^9 - 9 \lambda^8 \rho^5 \rho_1^5 \rho_2^7 \\
& + 12 \bar{h}^2 \lambda^6 \rho^4 \rho_1^6 \rho_2^5 \rho_4 - 60 \bar{h}^2 \lambda^6 \rho^4 \rho_1^6 \rho_2^4 \rho_3^2 - 104 \bar{h}^2 \lambda^6 \rho^4 \rho_1^5 \rho_2^6 \rho_3 - 93 \bar{h}^2 \lambda^6 \rho^4 \rho_1^4 \rho_2^8 \\
& + 3 \lambda^2 \rho^4 \rho_1^7 \rho_2^{10} \rho_3 + 92 \bar{h}^2 \lambda^6 \rho^3 \rho_1^6 \rho_2^5 \rho_3 + 64 \bar{h}^2 \lambda^6 \rho^3 \rho_1^5 \rho_2^7 + 3 \lambda^2 \rho^3 \rho_1^7 \rho_2^{11} + \bar{h}^2 \rho^2 \rho_1^7 \rho_2^{10} \rho_3 \\
& - 3 \lambda^2 \rho^2 \rho_1^8 \rho_2^{10} + \bar{h}^2 \rho \rho_1^7 \rho_2^{11} - \rho_1^8 \rho_2^{10} \bar{h}^2.
\end{aligned}$$

While deriving the above, we have used the dimensionless quantities

$$\rho = \frac{R}{B}, \quad \rho_1 = \frac{r^{(0)}}{B}, \quad \rho_2 = r^{(0)\prime}, \quad \rho_3 = r^{(0)\prime\prime} B, \quad \rho_4 = r^{(0)\prime\prime\prime} B^2, \quad \text{and} \quad \bar{h} = \frac{h}{B}. \quad (3.6)$$

The principal solution for $\lambda > 1$ allows the contraction of inner radius and expansion of outer radius of the plate which are investigated for two different boundary conditions. In the first boundary condition, we consider the inner boundary of the plate to be unconstrained or free to contract due to growth ($\lambda > 1$) and the outer boundary is constrained (IFOC¹). This condition is inspired from the behaviour of soft biological tissue such as skin where the wounded skin grows to close a wound (Swain and Gupta, 2015; Bowden et al., 2016). The second boundary condition models a constrained inner edge and unconstrained outer edge (ICOF²) of a plate where only the outer edge is allowed to deform during growth process. This condition is akin to the deformation of plants and soft polymeric material such as swollen gels (Mora and Boudaoud, 2006; Liu et al., 2013).

3.1.1 Case 1: Constrained outer boundary and unconstrained inner boundary

If the inner edge (at $\rho = A/B = A^*$) of the plate is free to contract or expand then the radial stress at inner edge on bottom and top surface is $P_{Rr}|_{Z=0} = P_{Rr}|_{Z=2h} = 0$ (which corresponds to $P_{Rr}^{(0)} = P_{Rr}^{(2)} = 0$ using (2.10)) and can further be rewritten in terms of dimensionless variables as

$$\lambda \left[\frac{2\rho_1}{\lambda} - \frac{2\lambda^5 A^{*2}}{\rho_1^2 \rho_2^3} \right] = 0, \quad (3.7a)$$

$$\begin{aligned}
& 8\rho_2^2 A^{*5} \lambda^6 \rho_3 + 4\rho_2 \rho_1 \rho_4 A^{*5} \lambda^6 - 4\rho_3^2 \rho_1 A^{*5} \lambda^6 - 8\rho_2^3 A^{*4} \lambda^6 - 4\rho_2 \rho_1 \rho_3 A^{*4} \lambda^6 + 2\rho_2^8 \rho_1 A^{*3} \\
& + 7\rho_2^6 \rho_1^2 A^{*3} \rho_3 + \rho_2^5 \rho_1^3 \rho_4 A^{*3} + 8\rho_1^4 \rho_3^2 \rho_2^2 A^{*3} + 8\rho_2^2 \rho_1 A^{*3} \lambda^6 + 3\rho_2^7 \rho_1^2 A^{*2} - \rho_2^5 \rho_1^3 \rho_3 A^{*2} \\
& - 15\rho_2^6 \rho_1^3 A^* - 6\rho_2^4 \rho_1^4 \rho_3 A^* + 10\rho_2^5 \rho_1^4 = 0.
\end{aligned} \quad (3.7b)$$

If the outer edge of the plate is constrained then the displacement of bottom and top surface at $\rho = 1$ is 0 i.e., $r^{(0)}(B) = B$, and $r^{(0)} + (2h)r^{(1)} + 2h^2r^{(2)} = B$ and is given by

$$\rho_1(1) = 1, \quad (3.8a)$$

$$r^{(2)}(1) = -2\rho_2^2 \lambda^6 - 2\rho_1 \rho_3 \lambda^6 + 2\rho_2 \rho_1 \lambda^6 - \rho_2^4 \rho_1^3 \rho_3 - \rho_2^5 \rho_1^3 + \rho_2^4 \rho_1^4 = 0. \quad (3.8b)$$

¹IFOC – Inner boundary of the plate is unconstrained (free) and outer boundary of the plate is constrained.

²ICOF – Inner boundary of the plate is constrained and the outer boundary of the plate is free.

3.1.2 Case 2: Constrained inner boundary and unconstrained outer boundary

If the inner edge of the plate is constrained then the displacement of bottom and top surface at the inner edge ($\rho|_{A^*} = 0$) is

$$r^{(0)}(A^*) = A^* \rightarrow \rho_1(A^*) = A^*, \quad (3.9a)$$

$$r^{(2)}(A^*) = -2\rho_2^2 A^{*4} \lambda^6 - 2\rho_1 \rho_3 A^{*4} \lambda^6 + 2\rho_2 \rho_1 A^{*3} \lambda^6 - \rho_2^4 \rho_1^3 \rho_3 A^{*2} - \rho_2^5 \rho_1^3 A^* + \rho_2^4 \rho_1^4 = 0. \quad (3.9b)$$

If the outer edge is unconstrained, the radial stress $P_{Rr}^{(0)} = P_{Rr}^{(2)} = 0$ at $\rho = 1$ is expressed as

$$\lambda \left[\frac{2\rho_1}{\lambda} - \frac{2\lambda^5}{\rho_1^2 \rho_2^3} \right] = 0, \quad (3.10a)$$

$$\begin{aligned} 8\rho_2^2 \lambda^6 \rho_3 + 4\rho_2 \rho_1 \rho_4 \lambda^6 - 4\rho_3^2 \rho_1 \lambda^6 - 8\rho_2^3 \lambda^6 - 4\rho_2 \rho_1 \rho_3 \lambda^6 + 2\rho_2^8 \rho_1 + 7\rho_2^6 \rho_1^2 \rho_3 + \rho_2^5 \rho_1^3 \rho_4 \\ + 8\rho_1^4 \rho_1^3 \rho_3^2 + 8\rho_2^2 \rho_1 \lambda^6 + 3\rho_2^7 \rho_1^2 - \rho_2^5 \rho_1^3 \rho_3 - 15\rho_2^6 \rho_1^3 - 6\rho_2^4 \rho_1^4 \rho_3 + 10\rho_2^5 \rho_1^4 = 0. \end{aligned} \quad (3.10b)$$

3.1.3 Numerical pre-buckling solution

In this section, we discuss the deformation associated with the principal solution (3.4) for both the boundary conditions. In the first case (IFOC), we numerically solve the system of ODEs (3.5) subjected to the boundary conditions (3.7) and (3.8). The numerical solutions for primary in-plane deformation of an annulus plate for different radius ratios $B/A = 1, 1.5, 2$ (see Figure 3) are obtained using the `bvp4c` solver available in Matlab. The dependence of deformed inner radius (a/A) on the growth parameter ($\lambda > 1$) for a plate of thickness $\bar{h} = 0.03$ is presented in Figure 3a. On the application of growth, the inner boundary of the annular plate contracts resulting in a decrease of the inner radius ($a < A$). The plate with a high radius ratio $B/A = 2$ shows more contraction even for a smaller value of λ compared to the other ratios. The numerical pre-buckling solution for the second case (ICOOF) is obtained by solving the system of ODEs (3.5) subjected to the boundary conditions (3.9) and (3.10). In this case, we have shown the variation of the deformed outer radius (b/B) with growth factor λ in Figure 3b. The outer edge of a plate expands as λ increases and plates with higher radius ratio show more expansion in comparison to plates with smaller radius ratio.

4 Linear bifurcation analysis

We derive the PDEs for onset of buckling in an isotropically growing annular plate. We seek a bifurcation solution close to the primary solution by using three different types of perturbation: (a) asymmetric perturbation along radial, circumferential and thickness directions (i.e, r, θ, z coordinates), (b) axisymmetric perturbation along radial and thickness directions (i.e, r, z coordinates, and (c) asymmetric perturbation along circumferential and thickness directions (i.e, θ, z coordinates).

4.1 Perturbation along radial, circumferential and thickness direction

Consider the following small asymmetric perturbations to the pre-buckling solution (3.4) scaled by a parameter $0 < \epsilon \ll 1$

$$\begin{aligned} r^{(0)}(R, \Theta) &= r(R) + \epsilon \Delta U(R) \cos(m\Theta), \\ \theta^{(0)}(R, \Theta) &= \Theta + \epsilon \Delta V(R) \sin(m\Theta), \\ z^{(0)}(R, \Theta) &= C_z + \epsilon \Delta W(R) \cos(m\Theta), \end{aligned} \quad (4.1)$$

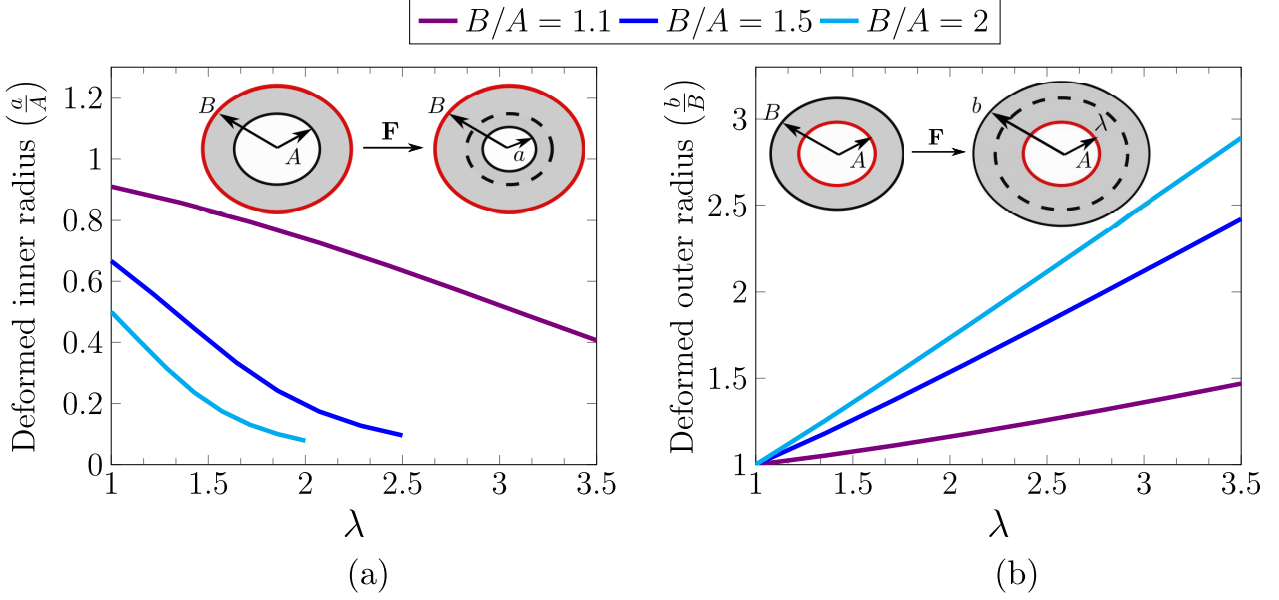


Figure 3: a) Dependence of the deformed inner radius (a/A) on growth factor λ at $\bar{h} = 0.03$ when outer edge of plate is constrained and inner edge is unconstrained (IFOC), and b) Dependence of deformed outer radius (b/B) on growth factor λ at $\bar{h} = 0.03$ when the inner edge of plate is constrained and the outer edge is unconstrained (ICOF).

where $m = 1, 2, 3, \dots$ represents the wave number in the circumferential direction and C_z is a constant that models rigid motion of the plate. Upon substituting (4.1) in the plate governing equation (2.11), we obtain ODEs in terms of dimensionless displacement functions U, V and W as

$$a_1 U'' + a_2 U' + a_3 U + a_4 V' + a_5 V + a_6 W''' + a_7 W'' + a_8 W' + a_9 W = 0, \quad (4.2a)$$

$$b_1 V'' + b_2 V' + b_3 V + b_4 U' + b_5 U + b_6 W'' + b_7 W' + b_8 W = 0, \quad (4.2b)$$

$$\begin{aligned} c_1 W'' + c_2 W' + c_3 W + c_4 U''' + c_5 U'' + c_6 U' + c_7 U + c_8 V'' + c_9 V' + c_{10} V \\ + c_{11} W^{iv} + c_{12} W''' + c_{13} W'' + c_{14} W' + c_{15} W = 0, \end{aligned} \quad (4.2c)$$

where $U = \Delta U/B$, $V = \Delta V/B$, and $W = \Delta W/B$. Equations. (4.2a) – (4.2c) are rewritten into a system of first order differential equations by substituting $[y_1, y_2, \dots, y_8] = [U, U', V, V', W, W', W'', W''']^T$ resulting in

$$\mathbf{H}\mathbf{Y}' = \mathbf{g}. \quad (4.3)$$

Here, $\mathbf{H} = \text{diag}(1, a_1, 1, b_1, 1, 1, 1, 1, c_{11})$ is an 8×8 matrix, and $\mathbf{Y}' = [y'_1, y'_2, y'_3, y'_4, y'_5, y'_6, y'_7, y'_8]^T$, and $\mathbf{g} = [y_1, y_2, y_3, y_4, y_5, y_6, y_7, y_8]^T$ are 8×1 column vectors. The coefficients in (4.2a) – (4.2c) are detailed in the supplementary document. The displacement boundary conditions for the IFOC case are

$$U'(A^*) = V(A^*) = W''(A^*) = W'''(A^*) = 0, \quad (4.4a)$$

$$U(1) = V(1) = W(1) = W'(1) = 0, \quad (4.4b)$$

and for the ICOF case are

$$U(A^*) = V(A^*) = W(A^*) = W'(A^*) = 0, \quad (4.5a)$$

$$U'(1) = V(1) = W''(1) = W'''(1) = 0. \quad (4.5b)$$

Here, equations (4.4a) (respectively, (4.5b)) correspond to unconstrained inner edge (respectively, outer edge) of annular plate which allows contraction (respectively, expansion) and no restriction of bending moment ($W'' = 0$) and transverse shear ($W''' = 0$). Equations (4.4b) and (4.5a) correspond to clamped (constrained) outer and inner edges of the plate, respectively.

4.1.1 Perturbation along radial and thickness direction

In this case, the linear bifurcation analysis is performed by perturbing the principal solution (3.4) axisymmetrically with a small parameter $0 < \epsilon \ll 1$ by using the following ansatz

$$r^{(0)}(R, \Theta) = r(R) + \epsilon \Delta U(R) \cos(m\Theta), \quad \theta^{(0)} = \Theta, \quad z^{(0)}(R, \Theta) = C_z + \epsilon \Delta W(R) \cos(m\Theta), \quad (4.6)$$

where ‘ m ’ is again an integer representing the wave number in the circumferential direction. On substituting (4.6) in the plate governing equation (2.11), we obtain ODEs in terms of the dimensionless displacement functions U and W which one can simply obtain by setting coefficients $a_4 = a_5 = 0$ in (4.2a) and $c_8 = c_9 = c_{10} = 0$ in (4.2c). The system (4.2) is now reduced to two ODEs which is further simplified into six first-order linear differential equations of the form

$$\mathbf{m}' = \mathbf{B}\mathbf{m}, \quad (4.7)$$

where $\mathbf{m} = [U, U', W, W', W'', W''']$ and $\mathbf{B} = \text{diag}(1, a_1, 1, 1, 1, c_{11})$. The IFOC boundary condition is given as

$$U'(A^*) = W''(A^*) = W'''(A^*) = 0, \quad \text{and} \quad U(1) = W(1) = W'(1) = 0, \quad (4.8)$$

and the ICOF condition associated with this type of perturbation yields

$$U(A^*) = W(A^*) = W'(A^*) = 0, \quad \text{and} \quad U'(1) = W''(1) = W'''(1) = 0. \quad (4.9)$$

4.1.2 Perturbation along circumferential and thickness direction

In this case, the bifurcation solution is obtained by applying an asymmetric perturbation to the principal solution along circumferential and thickness directions using the following ansatz

$$r^{(0)}(R) = r(R), \quad \theta^{(0)}(R, \Theta) = \Theta + \epsilon \Delta V(R) \sin(m\Theta), \quad \text{and} \quad z^{(0)}(R, \Theta) = C_z + \epsilon \Delta W(R) \cos(m\Theta), \quad (4.10)$$

where $m = 1, 2, 3 \dots$ represents the circumferential wave number. In this type of perturbation, the incremental elastic strain is dependent on the Θ - Z coordinates. Thus, the incremental ODEs are obtained in terms of dimensionless displacement functions V and W by substituting (4.10) in (2.11) or we can obtain these ODEs by setting the coefficients $b_4 = b_5 = 0$ in (4.2b) and $c_4 = c_5 = c_6 = c_7 = 0$ in (4.2c). The resulting three equations in the system (4.3) is again reduced to two ODEs which further can be rewritten in the form of

$$\mathbf{t}' = \mathbf{K}\mathbf{t} \quad (4.11)$$

where $\mathbf{t} = [V, V', W, W', W'', W''']$ and $\mathbf{K} = \text{diag}(1, b_1, 1, 1, 1, c_{11})$. The IFOC boundary conditions for this case are

$$V(A^*) = W''(A^*) = W'''(A^*) = 0, \quad \text{and} \quad V(1) = W(1) = W'(1) = 0. \quad (4.12)$$

The ICOF boundary conditions are given by

$$V(A^*) = W(A^*) = W'(A^*) = 0, \quad \text{and} \quad V(1) = W''(1) = W'''(1) = 0. \quad (4.13)$$

5 Result and analysis

The previous Section 4 discussed the possible type of perturbations (axisymmetry and asymmetric), corresponding ODEs and boundary conditions for the stability analysis. In this section, we numerically solve the derived ODEs to determine the critical growth factor at the onset of bifurcation. The numerical strategy used to derive the bifurcation solution was detailed in Section 5.1. We have shown only one set of bifurcation solutions in Subsection 5.1.1 when a plate is perturbed in R - Θ - Z direction and subjected to IFOC boundary condition. This is to illustrate the stability of buckling solution of the growing plate when perturbed. Then in Section 5.2, we compare the bifurcation solution of each type of perturbation considered in Section 4 and investigate the desired type of perturbation that result in energetically preferred bifurcation solution. In the next Section 5.3, we have shown the comparison of preferred bifurcation solution for both boundary conditions.

5.1 Numerical scheme of bifurcation analysis for growing annular plate

In this section, we numerically solve the ODEs obtained in Section 4.1 for the critical growth factor (λ_{cr}) responsible for the onset of instability. The numerical solutions of the resulting boundary value problems (BVPs) are computed using the compound matrix method (Haughton and Orr, 1997; Mehta et al., 2021b) as well as the standard shooting method or determinant method (Haughton and Ogden, 1979; Saxena, 2018). Both the numerical methods are implemented in Matlab 2018a and the computed results are the same. However, the compound matrix method is much faster than the shooting method (Mehta et al., 2021a). Equations are integrated using the `ode45` ODE solver that implements an explicit Runge-Kutta method and then the `fminsearchbnd` optimisation subroutine (D'Errico, 2021) based on Nelder-Mead simplex algorithm is used to minimise the errors.

5.1.1 Bifurcation solution for a plate with clamped outer edge condition

In this section, we evaluated the value of λ_{cr} for the first case as discussed in 4.1 i.e., perturbation along R - Θ - Z direction to demonstrate the behaviour of bifurcation solution for an annular plate. For this, we numerically solve the system (4.3) subjected to IFOC boundary condition (4.4). The dependence of λ_{cr} on the plate thickness (\bar{h}) with different radius ratios $B/A = 1.1, 1.5, 2$ at various circumferential wavenumber (m) is shown in Figure 4. The λ_{cr} monotonically increases with \bar{h} suggests that thicker plates require higher value of growth to cause wrinkling instability. Furthermore, the magnitude of λ_{cr} decreases with the increase of B/A due to an apparent decrease in bending stiffness of the plate. We also observe that the critical wavenumber (m_{cr}) depends on the thickness and radius ratio of the plate. The higher modes are energetically preferred for the low B/A value whereas the lower modes are stable with the increasing value of B/A . For a plate with smaller radius ratio, $B/A = 1.1$, the obtained critical wavenumber is $m_{cr} = 22$ in the thin regime ($0.05 < \bar{h} < 0.1$), and $m_{cr} = 23$ in the thick regime ($\bar{h} > 0.1$). However, for $B/A = 1.5$ and 2, the critical wavenumbers are $m_{cr} = 4$ and $m_{cr} = 2$, respectively.

5.2 Comparison of axisymmetric and asymmetric bifurcation solutions

Here, we compare the bifurcation solutions of axisymmetric and asymmetric perturbations as discussed in Section 4.1.1 and 4.1.2, respectively. The λ_{cr} is calculated by numerically solving the systems (4.7) and (4.11) subjected to the IFOC boundary conditions (4.8) and (4.12), respectively using the compound matrix method. Table 1 shows the dependence of λ_{cr} on plate thickness (\bar{h}) and plate radius ratio (B/A) at the corresponding critical mode number (m_{cr}) for each type of considered perturbation. The bifurcation solution corresponding to axisymmetric (i.e., along R - Z) and asymmetric (i.e., along

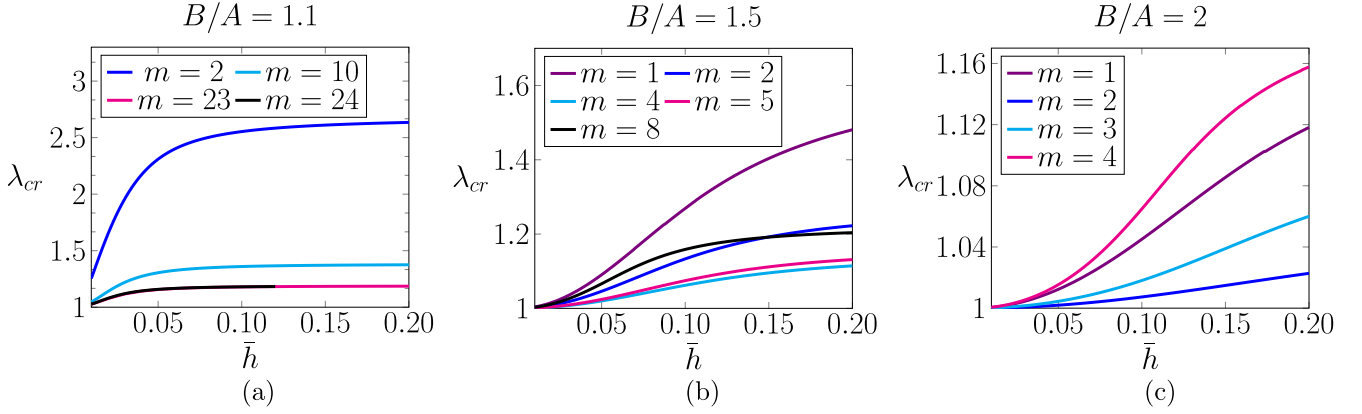


Figure 4: Dependence of critical growth factor on thickness of plate (\bar{h}) for various aspect ratios a) $B/A = 1.1$, b) $B/A = 1.5$, and c) $B/A = 2$ using radial-hoop-thickness direction perturbation ansatz.

Table 1: Comparison of dependence of critical growth factor on dimensionless plate thickness ($\bar{h} = 0.03, 0.05, 0.1, 0.15, 0.2$) at critical circumferential wavenumber (m_{cr}) for plate radius ratio, $B/A = 1.1, 1.5, 2$. The critical value of growth function is obtained for both axisymmetric and asymmetric perturbations to principal solution. The highlighted values represent the lowest value of λ_{cr} obtained at m_{cr} for preferred bifurcation solution.

$B/A = 1.1$			$B/A = 1.5$			$B/A = 2$		
λ_{cr} (R-Z)	λ_{cr} (Θ -Z)	λ_{cr} (R- Θ -Z)	λ_{cr} (R-Z)	λ_{cr} (Θ -Z)	λ_{cr} (R- Θ -Z)	λ_{cr} (R-Z)	λ_{cr} (Θ -Z)	λ_{cr} (R- Θ -Z)
1.2106 ($m_{cr} = 16$)	1.1154 ($m_{cr} = 20$)	1.1127 ($m_{cr} = 20$)	1.0077 ($m_{cr} = 4$)	1.0074 ($m_{cr} = 4$)	1.0076 ($m_{cr} = 4$)	1.0007 ($m_{cr} = 2$)	1.0007 ($m_{cr} = 2$)	1.0007 ($m_{cr} = 2$)
1.4604 ($m_{cr} = 13$)	1.1619 ($m_{cr} = 22$)	1.1547 ($m_{cr} = 21$)	1.0214 ($m_{cr} = 4$)	1.0191 ($m_{cr} = 4$)	1.0200 ($m_{cr} = 4$)	1.0019 ($m_{cr} = 2$)	1.0019 ($m_{cr} = 2$)	1.0019 ($m_{cr} = 2$)
1.7893 ($m_{cr} = 10$)	1.1901 ($m_{cr} = 23$)	1.1793 ($m_{cr} = 22$)	1.0810 ($m_{cr} = 4$)	1.0551 ($m_{cr} = 4$)	1.0621 ($m_{cr} = 4$)	1.0075 ($m_{cr} = 2$)	1.0063 ($m_{cr} = 2$)	1.0073 ($m_{cr} = 2$)
1.8838 ($m_{cr} = 9$)	1.1959 ($m_{cr} = 24$)	1.1843 ($m_{cr} = 23$)	1.1477 ($m_{cr} = 4$)	1.0814 ($m_{cr} = 4$)	1.0955 ($m_{cr} = 4$)	1.0156 ($m_{cr} = 2$)	1.0113 ($m_{cr} = 2$)	1.0148 ($m_{cr} = 2$)
1.9162 ($m_{cr} = 9$)	1.1979 ($m_{cr} = 24$)	1.1860 ($m_{cr} = 23$)	1.1849 ($m_{cr} = 3$)	1.0962 ($m_{cr} = 4$)	1.1144 ($m_{cr} = 4$)	1.0247 ($m_{cr} = 2$)	1.0155 ($m_{cr} = 2$)	1.0228 ($m_{cr} = 2$)

Θ -Z) perturbations to principal solution (3.4) show a similar trend in comparison with the bifurcation solution obtained in Section 5.1.1. The bifurcation solution corresponding to axisymmetric perturbation results in high λ_{cr} , thus requiring higher growth factor as compared to bifurcation solution associated with asymmetric perturbations. For a plate with $B/A = 1.5, 2$, the bifurcation solution obtained by perturbing Θ -Z direction have minimum energy as shown in Table 1 (highlighted value correspond to lowest value of λ_{cr} for preferred bifurcation solution) suggesting that the asymmetrically perturbed solution is energetically preferred. Whereas, for a plate with low radius ratio $B/A = 1.1$, the bifurcation solution obtained by perturbation along R- Θ -Z direction have lower energy, however the result is very close to the solution obtained by Θ -Z perturbation. This comparison conclude that the Θ -Z (asymmetric) type of perturbation is appropriate for the hyperelastic annular plate with moderate and high radius ratio when subjected to IFOC condition as compared to other perturbations.

Table 2: Dependence of the critical value of growth factor (λ_{cr}) on plate thickness (\bar{h}) and critical wavenumber (m_{cr}). The λ_{cr} is obtained for the plate aspect ratio $B/A = 1.1, 1.5, 2$ at various \bar{h} subjected to IFOC and ICOF boundary conditions.

\bar{h}	$B/A = 1.1$		$B/A = 1.5$		$B/A = 2$	
	λ_{cr} (IFOC)	λ_{cr} (ICOF)	λ_{cr} (IFOC)	λ_{cr} (ICOF)	λ_{cr} (IFOC)	λ_{cr} (ICOF)
0.03	1.1127 ($m_{cr} = 20$) ($R\Theta Z$)	1.1327 ($m_{cr} = 23$) ($R\Theta Z$)	1.0074 ($m_{cr} = 4$) (ΘZ)	1.0386 ($m_{cr} = 6$) ($R\Theta Z$)	1.0007 ($m_{cr} = 2$) (ΘZ)	1.0306 ($m_{cr} = 4$) ($R\Theta Z$)
	1.1547 ($m_{cr} = 21$) ($R\Theta Z$)	1.1680 ($m_{cr} = 26$) ($R\Theta Z$)	1.0191 ($m_{cr} = 4$) (ΘZ)	1.0816 ($m_{cr} = 6$) ($R\Theta Z$)	1.0019 ($m_{cr} = 2$) (ΘZ)	1.0681 ($m_{cr} = 4$) ($R\Theta Z$)
0.05	1.1793 ($m_{cr} = 22$) ($R\Theta Z$)	1.1850 ($m_{cr} = 30$) ($R\Theta Z$)	1.0551 ($m_{cr} = 4$) (ΘZ)	1.1493 ($m_{cr} = 7$) ($R\Theta Z$)	1.0063 ($m_{cr} = 2$) (ΘZ)	1.1387 ($m_{cr} = 5$) ($R\Theta Z$)
	1.1843 ($m_{cr} = 23$) ($R\Theta Z$)	1.1879 ($m_{cr} = 32$) ($R\Theta Z$)	1.0814 ($m_{cr} = 4$) (ΘZ)	1.1690 ($m_{cr} = 9$) ($R\Theta Z$)	1.0113 ($m_{cr} = 2$) (ΘZ)	1.1624 ($m_{cr} = 6$) ($R\Theta Z$)
0.1	1.1860 ($m_{cr} = 23$) ($R\Theta Z$)	1.1888 ($m_{cr} = 48$) ($R\Theta Z$)	1.0962 ($m_{cr} = 4$) (ΘZ)	1.1727 ($m_{cr} = 14$) ($R\Theta Z$)	1.0155 ($m_{cr} = 2$) (ΘZ)	1.1705 ($m_{cr} = 6$) ($R\Theta Z$)

5.3 Comparison of buckling solution of a plate subjected to both boundary conditions

In this section, we evaluate the λ_{cr} for an annular plate considering all type of perturbations by numerically solving (4.3), (4.7), and (4.11) subjected to ICOF conditions (4.5), (4.9), and (4.13), respectively. The values of λ_{cr} obtained using the compound matrix method (or shooting method) are compared for each type of perturbation and then we collect the lowest preferred values of λ_{cr} (at m_{cr}) corresponding to preferred bifurcation solutions. Table 2 shows the dependence of preferred bifurcation solution (lowest λ_{cr}) on plate thickness (\bar{h}) and radius ratio B/A when the growing plate is subjected to ICOF boundary condition. This table also compares the lowest values of λ_{cr} of the plate subjected to IFOC condition (highlighted in Table 1) with the obtained ICOF results. We observe that the variation of λ_{cr} with plate thickness (\bar{h}) and radius ratio (B/A) for both the boundary conditions is quite similar. The value of m_{cr} and λ_{cr} increases with \bar{h} for a fixed B/A which suggest more wrinkles in hoop direction are observed for thicker plates at high value of λ_{cr} . Further, we observe that the plate subjected to ICOF boundary condition, the bifurcation solution associated with $R\Theta Z$ perturbation have minimum energy as compared to other type of perturbations. In addition, the magnitude of λ_{cr} and m_{cr} is higher for the bifurcation solution associated with ICOF case when compared to IFOC. For the same geometric parameters $B/A = 1.5$ and $\bar{h} = 0.1$, the value of λ_{cr} associated with IFOC condition is 1.0551 at $m_{cr} = 4$ and ICOF condition is $\lambda_{cr} = 1.1493$ at $m_{cr} = 7$. Next, we discuss these results in context of stress and displacement plots.

5.3.1 Stress and displacement distribution at bifurcation

In this section, we present the spatial distribution of stress and displacements to provide a physical understanding of the bifurcation solution. The dimensionless average stress distribution along the

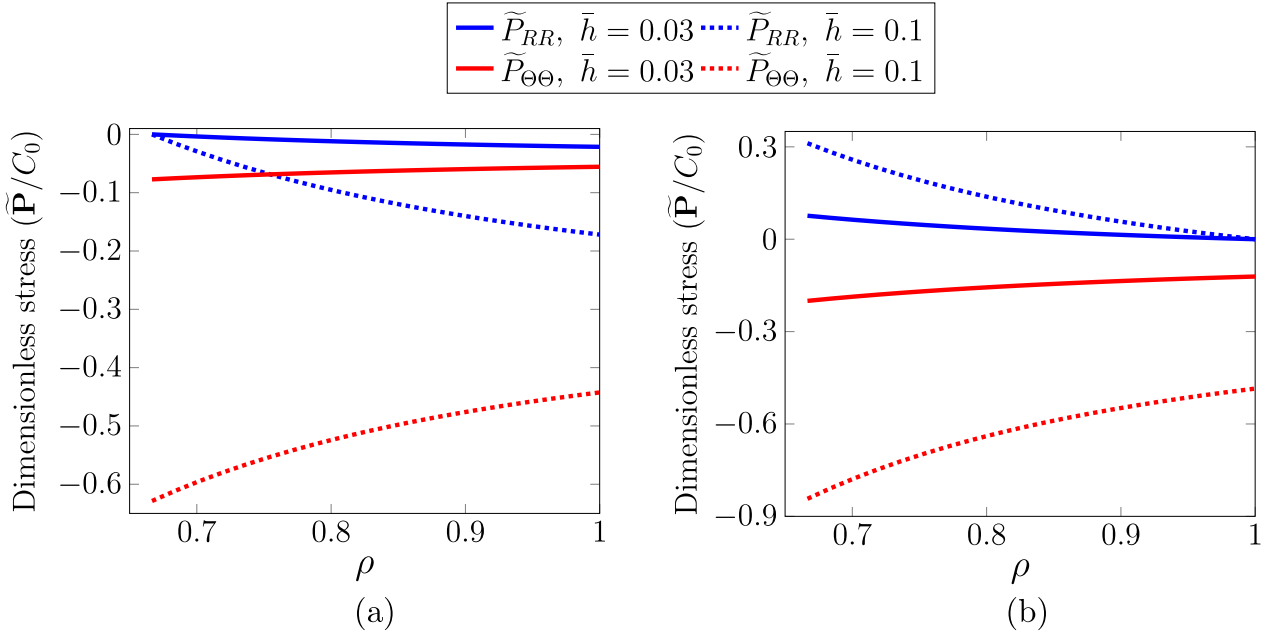


Figure 5: The dimensionless average Piola-Kirchhoff stress is plotted against dimensionless radius (ρ) of the annular plate subjected to (a) IFOC, and (b) ICOF. The blue and red curve represents the radial ($\tilde{P}_{\text{rad}}/C_0 = \tilde{P}_{RR}$) and hoop ($\tilde{P}_{\text{hoop}}/C_0 = \tilde{P}_{\Theta\Theta}$) stress distribution, respectively along the radius. The solid stress distribution curves correspond to the plate thickness, $\bar{h} = 0.03$ and dotted stress distribution curves are associated with the plate thickness, $\bar{h} = 0.1$.

radius of annular plate (for $\bar{h} = 0.03, 0.1$) associated with both the boundary conditions is presented in Figure 5. For a plate with fixed radius ratio $B/A = 1.5$ subjected to IFOC boundary condition i.e., (3.7) and (3.8) having $\lambda_{cr} = 1.0074$ (at $m_{cr} = 4, \bar{h} = 0.03$), the resulting dimensionless stress is compressive in the radial as well as circumferential direction as shown in Figure 5a. The blue solid curve represents the dimensionless radial stress (\tilde{P}_{RR}) which is zero at the inner edge and negative at the constrained outer edge of a plate. Whereas, the red solid curve correspond to dimensionless hoop stress ($\tilde{P}_{\Theta\Theta}$) which is negative (compressive) throughout the plate [Mathematical expressions for stresses are detailed in the supplementary document]. $\tilde{P}_{\Theta\Theta}$ is maximum (compressive) at the inner edge, and minimum (compressive) at the outer edge of the plate that causes wrinkling in circumferential direction at the inner unconstrained edge. For a plate $B/A = 1.5, m_{cr} = 6, \bar{h} = 0.03$, and $\lambda_{cr} = 1.0386$ subjected to ICOF boundary condition i.e., (3.9) and (3.10), the \tilde{P}_{RR} is tensile at inner edge and zero at the free outer edge as shown in Figure 5b. The $\tilde{P}_{\Theta\Theta}$ is maximum (compressive) at inner edge due to constrained boundary condition and minimum (compressive) at free outer edge of a plate which causes wrinkling in circumferential direction. We observe that for IFOC condition, both the \tilde{P}_{RR} and $\tilde{P}_{\Theta\Theta}$ are compressive which promotes the bifurcation where as for ICOF boundary condition, $\tilde{P}_{\Theta\Theta}$ is compressive and \tilde{P}_{RR} is tensile that delays the bifurcation. Due to this, higher compressive stresses are required to form a wrinkled pattern in circumferential direction when plate is subjected to ICOF boundary condition. We have also shown the stress distribution for thick plate for both cases. The dotted curves represents the stress distribution for a plate of $B/A = 1.5, \bar{h} = 0.1$ having $\lambda_{cr} = 1.0551$, and 1.1493 corresponding to first (see Figure 5a) and second (see Figure 5b) boundary condition case, respectively. The stress distribution in thick plate shows the similar behaviour in contrast to thin plate, however the stress (radial as well as hoop) magnitude are higher in thick plates.

Next, we present the planar displacement distribution in the deformed coordinate system. We demonstrate the out-of-plane contour plot using (4.1) and (4.10) for the annular plate of $B/A =$

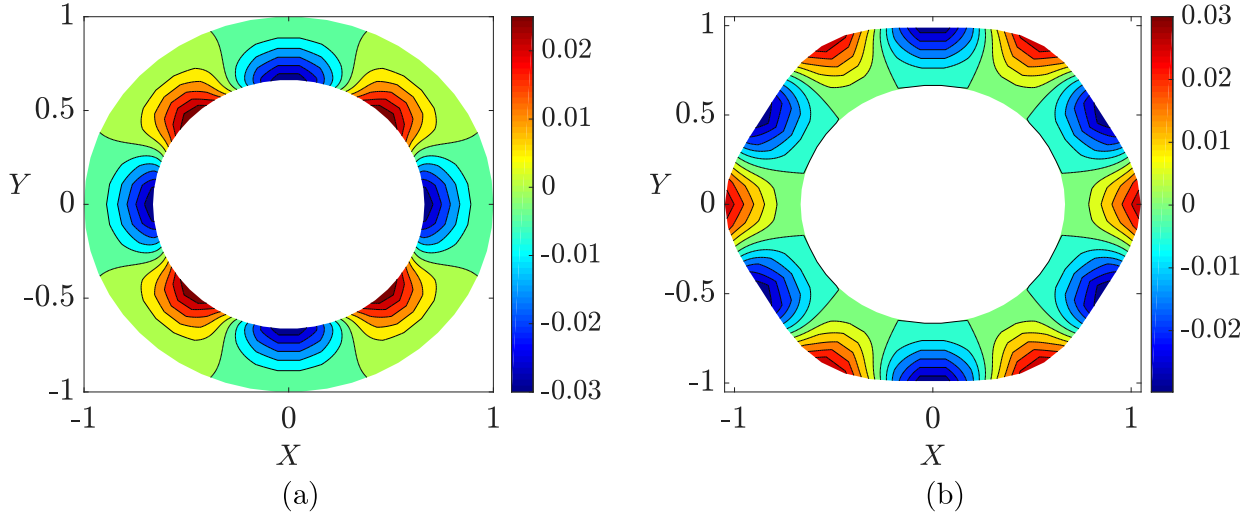


Figure 6: Contour plots of normalised out-of-plane displacement for an annular plate with $B/A = 1.5$, $\bar{h} = 0.03$ at critical wavenumber. A planar view of the annular plate in its deformed configuration is presented which is subjected to (a) IFOC at $m_{cr} = 4$, $\lambda_{cr} = 1.0074$, and (b) ICOF at $m_{cr} = 6$, $\lambda_{cr} = 1.0386$.

1.5, $\bar{h} = 0.03$ subjected to ICOF and IFOC boundary conditions, respectively in Figure 6. For this, we have used the parameters $\epsilon \sim \bar{h}$, $C_z = 0$. The numerical solution is obtained by solving (4.3) with $\lambda_{cr} = 1.0386$, $m_{cr} = 6$ and (4.11) with $\lambda_{cr} = 1.0074$, $m_{cr} = 4$ (see Table 2) subjected to (4.4) and (4.12), respectively using `bvp4c` subroutine in Matlab. The normalised out-of-plane displacement is maximum at the unconstrained inner edge and zero at the clamped outer edge of the annular plate when using IFOC condition as shown in Figure 6a. This suggests that the circumferential wrinkling modes occur at the inner unconstrained edge. Since the outer edge is free in ICOF boundary condition, the normalised out-of-plane displacement is maximum at the outer edge (representing the circumferential wrinkling modes) which reduced to zero at the clamped inner edge of the plate as shown in Figure 6b.

6 Conclusion

In this work, we investigated the wrinkling in a growing hyperelastic annular plate using finite strain asymptotic plate theory. A 3-D plate equilibrium system is reduced to 2-D plate governing system by adopting series expansion along thickness direction. A homogeneous isotropic growth function is considered as a control parameter in inducing the circumferential instability in an incompressible neo-Hookean annular plate. We perform the linear stability analysis with asymmetric (i.e., along R - Θ - Z and Θ - Z direction) as well as axisymmetric perturbations (i.e., along R - Z direction) subjected to two cases of boundary conditions, IFOC and ICOF. The numerical solution of resulting system of incremental differential equations in each case is obtained using compound matrix method. The critical value for growth function (λ_{cr}) at critical wavenumber (m_{cr}) is evaluated for each type of perturbation and boundary conditions. We observe that the bifurcation solution corresponding to axisymmetric perturbation subjected to both boundary conditions is undesirable as it has high value of λ_{cr} suggesting higher energy in contrast to solution associated with asymmetric perturbations. Further, the bifurcation solution obtained by Θ - Z perturbation subjected to IFOC boundary condition results in lower value of λ_{cr} for all plate thickness values, hence energetically preferred. However, for the plate with low radius ratio $B/A = 1.1$, the R - Θ - Z perturbation is preferred for a stable buckling solution. The m_{cr} has high

value for low and low value for high plate radius ratio suggesting that higher modes in circumferential direction are stable for low B/A while lower modes are preferred for the plate with high B/A . The magnitude of λ_{cr} increases monotonically with \bar{h} implying thicker plate is more stable as it buckles at higher values of λ_{cr} . Then the obtained solution is compared with the solution associated with ICOF boundary condition. It has been observed that both the bifurcation solutions exhibit a similar behaviour for variation of λ_{cr} (at m_{cr}) with B/A and \bar{h} , however the magnitude of λ_{cr} is higher using ICOF boundary condition due to generation of tensile radial stresses. In addition, the bifurcation solution obtained for the annular plate with $R\Theta Z$ perturbation is preferred throughout using ICOF boundary condition.

The current work is confined to analysing the wrinkling induce due to isotropic (and homogeneous) growth function in evolving systems, however they are generally considered as anisotropic (and inhomogeneous) which leads to irregular patterns. These avenues are now being investigated and our finding will be reported in a proper forum at a later stage.

Acknowledgements

Prashant Saxena acknowledges the financial support of the EPSRC grant no. EP/V030833/1.

References

Ambrosi D., Ateshian G.A., Arruda E.M., Cowin S., Dumais J., Goriely A., Holzapfel G.A., Humphrey J.D., Kemkemer R., Kuhl E. et al. “Perspectives on biological growth and remodeling”. *Journal of the Mechanics and Physics of Solids*, 59(4):863–883 (2011)

Balbi V. and Ciarletta P. “Morpho-elasticity of intestinal villi”. *Journal of the Royal Society Interface*, 10(82):20130109 (2013)

Ben Amar M. and Goriely A. “Growth and instability in elastic tissues”. *Journal of the Mechanics and Physics of Solids*, 53(10):2284–2319 (2005)

Bowden L., Byrne H., Maini P., and Moulton D. “A morphoelastic model for dermal wound closure”. *Biomechanics and modeling in mechanobiology*, 15(3):663–681 (2016)

Budday S., Steinmann P., and Kuhl E. “The role of mechanics during brain development”. *Journal of the Mechanics and Physics of Solids*, 72:75–92 (2014)

Cao Y., Jiang Y., Li B., and Feng X. “Biomechanical modeling of surface wrinkling of soft tissues with growth-dependent mechanical properties”. *Acta Mechanica Solida Sinica*, 25(5):483–492 (2012)

Cerda E. “Mechanics of scars”. *Journal of biomechanics*, 38(8):1598–1603 (2005)

Coen E., Rolland-Lagan A.G., Matthews M., Bangham J.A., and Prusinkiewicz P. “The genetics of geometry”. *Proceedings of the National Academy of Sciences*, 101(14):4728–4735 (2004)

Coman C.D. and Haughton D. “Localized wrinkling instabilities in radially stretched annular thin films”. *Acta Mechanica*, 185(3):179–200 (2006)

Coman C.D., Matthews M.T., and Bassom A.P. “Asymptotic phenomena in pressurized thin films”. *Proceedings of the Royal Society A: Mathematical, Physical and Engineering Sciences*, 471(2182):20150471 (2015)

Dai H.H. and Liu Y. “Critical thickness ratio for buckled and wrinkled fruits and vegetables”. *EPL (Europhysics Letters)*, 108(4):44003 (2014)

Dai H.H. and Song Z. “On a consistent finite-strain plate theory based on three-dimensional energy principle”. *Proceedings of the Royal Society A: Mathematical, Physical and Engineering Sciences*, 470(2171):20140494 (2014)

D’Errico J. “fminsearchbnd, fminsearchcon (<https://www.mathworks.com/matlabcentral/fileexchange/8277-fminsearchbnd-fminsearchcon>)”, MATLAB Central File Exchange.” (2021)

Dervaux J., Ciarletta P., and Ben Amar M. “Morphogenesis of thin hyperelastic plates: a constitutive theory of biological growth in the föppl–von kármán limit”. *Journal of the Mechanics and Physics of Solids*, 57(3):458–471 (2009)

Dortdivanlioglu B., Javili A., and Linder C. “Computational aspects of morphological instabilities using isogeometric analysis”. *Computer Methods in Applied Mechanics and Engineering*, 316:261–279 (2017)

Du P., Dai H.H., Wang J., and Wang Q. “Analytical study on growth-induced bending deformations of multi-layered hyperelastic plates”. *International Journal of Non-Linear Mechanics*, 119:103370 (2020)

Garikipati K., Arruda E.M., Grosh K., Narayanan H., and Calve S. “A continuum treatment of growth in biological tissue: the coupling of mass transport and mechanics”. *Journal of the Mechanics and Physics of Solids*, 52(7):1595–1625 (2004)

Goriely A. *The mathematics and mechanics of biological growth*, volume 45. Springer (2017)

Goriely A. and Ben Amar M. “Differential growth and instability in elastic shells”. *Physical review letters*, 94(19):198103 (2005)

Goriely A. and Ben Amar M. “On the definition and modeling of incremental, cumulative, and continuous growth laws in morphoelasticity”. *Biomechanics and modeling in mechanobiology*, 6(5):289–296 (2007)

Haughton D. and Ogden R. “Bifurcation of inflated circular cylinders of elastic material under axial loading—ii. exact theory for thick-walled tubes”. *Journal of the Mechanics and Physics of Solids*, 27(5-6):489–512 (1979)

Haughton D. and Orr A. “On the eversion of compressible elastic cylinders”. *International journal of solids and structures*, 34(15):1893–1914 (1997)

Ionov L. “Biomimetic hydrogel-based actuating systems”. *Advanced Functional Materials*, 23(36):4555–4570 (2013)

Kadapa C., Li Z., Hossain M., and Wang J. “On the advantages of mixed formulation and higher-order elements for computational morphoelasticity”. *Journal of the Mechanics and Physics of Solids*, 148:104289 (2021)

Kempaiah R. and Nie Z. “From nature to synthetic systems: shape transformation in soft materials”. *Journal of Materials Chemistry B*, 2(17):2357–2368 (2014)

Khang D.Y., Rogers J.A., and Lee H.H. “Mechanical buckling: mechanics, metrology, and stretchable electronics”. *Advanced Functional Materials*, 19(10):1526–1536 (2009)

Kienzler R. “On consistent plate theories”. *Archive of Applied Mechanics*, 72(4):229–247 (2002)

Kuhl E. “Growing matter: a review of growth in living systems”. *Journal of the Mechanical Behavior of Biomedical Materials*, 29:529–543 (2014)

Li B., Cao Y.P., Feng X.Q., and Gao H. “Mechanics of morphological instabilities and surface wrinkling in soft materials: a review”. *Soft Matter*, 8(21):5728–5745 (2012)

Li B., Huang S.Q., and Feng X.Q. “Buckling and postbuckling of a compressed thin film bonded on a soft elastic layer: a three-dimensional analysis”. *Archive of Applied Mechanics*, 80(2):175–188 (2010)

Li Z., Wang Q., Du P., Kadapa C., Hossain M., and Wang J. “Analytical study on growth-induced axisymmetric deformations and shape-control of circular hyperelastic plates”. *International Journal of Engineering Science*, 170:103594 (2022)

Liang H. and Mahadevan L. “The shape of a long leaf”. *Proceedings of the National Academy of Sciences*, 106(52):22049–22054 (2009)

Limbert G. and Kuhl E. “On skin microrelief and the emergence of expression micro-wrinkles”. *Soft matter*, 14(8):1292–1300 (2018)

Liu R.C., Liu Y., and Cai Z. “Influence of the growth gradient on surface wrinkling and pattern transition in growing tubular tissues”. *Proceedings of the Royal Society of London Series A*, 477(2254):20210441 (2021)

Liu Y., Ma W., and Dai H.H. “On a consistent finite-strain plate model of nematic liquid crystal elastomers”. *Journal of the Mechanics and Physics of Solids*, 145:104169 (2020a)

Liu Y., Zhang Z., Devillanova G., and Cai Z. “Surface instabilities in graded tubular tissues induced by volumetric growth”. *International Journal of Non-Linear Mechanics*, 127:103612 (2020b)

Liu Z., Swaddiwudhipong S., and Hong W. “Pattern formation in plants via instability theory of hydrogels”. *Soft Matter*, 9(2):577–587 (2013)

Mehta S., Raju G., Kumar S., and Saxena P. “Instabilities in a compressible hyperelastic cylindrical channel due to internal pressure and external constraints” (2021a)

Mehta S., Raju G., and Saxena P. “Growth induced instabilities in a circular hyperelastic plate”. *International Journal of Solids and Structures*, 226:111026 (2021b)

Mihai L.A. and Goriely A. “A plate theory for nematic liquid crystalline solids”. *Journal of the Mechanics and Physics of Solids*, 144:104101 (2020)

Mora T. and Boudaoud A. “Buckling of swelling gels”. *The European Physical Journal E*, 20(2):119–124 (2006)

Nassar D., Letavernier E., Baud L., Aractingi S., and Khosrotehrani K. “Calpain activity is essential in skin wound healing and contributes to scar formation”. *PloS one*, 7(5):e37084 (2012)

Papastavrou A., Steinmann P., and Kuhl E. “On the mechanics of continua with boundary energies and growing surfaces”. *Journal of the Mechanics and Physics of Solids*, 61(6):1446–1463 (2013)

Raybaud C. and Widjaja E. "Development and dysgenesis of the cerebral cortex: malformations of cortical development". *Neuroimaging Clinics*, 21(3):483–543 (2011)

Rodriguez E.K., Hoger A., and McCulloch A.D. "Stress-dependent finite growth in soft elastic tissues". *Journal of biomechanics*, 27(4):455–467 (1994)

Rogers J.A., Someya T., and Huang Y. "Materials and mechanics for stretchable electronics". *science*, 327(5973):1603–1607 (2010)

Saxena P. "Finite deformations and incremental axisymmetric motions of a magnetoelastic tube". *Mathematics and Mechanics of Solids*, 23(6):950–983 (2018)

Steele C.R. "Shell stability related to pattern formation in plants". *Journal of Applied Mechanics*, 67(2):237–247 (2000)

Stein-Montalvo L., Costa P., Pezzulla M., and Holmes D.P. "Buckling of geometrically confined shells". *Soft Matter*, 15(6):1215–1222 (2019)

Swain D. and Gupta A. "Interfacial growth during closure of a cutaneous wound: stress generation and wrinkle formation". *Soft matter*, 11(32):6499–6508 (2015)

Swain D. and Gupta A. "Mechanics of cutaneous wound rupture". *Journal of biomechanics*, 49(15):3722–3730 (2016)

Terwagne D., Brojan M., and Reis P.M. "Smart morphable surfaces for aerodynamic drag control". *Advanced materials*, 26(38):6608–6611 (2014)

Vandiver R. and Goriely A. "Differential growth and residual stress in cylindrical elastic structures". *Philosophical Transactions of the Royal Society A: Mathematical, Physical and Engineering Sciences*, 367(1902):3607–3630 (2009)

Wang F.F., Steigmann D.J., and Dai H.H. "On a uniformly-valid asymptotic plate theory". *International Journal of Non-Linear Mechanics*, 112:117–125 (2019a)

Wang J., Song Z., and Dai H.H. "On a consistent finite-strain plate theory for incompressible hyperelastic materials". *International Journal of Solids and Structures*, 78:101–109 (2016)

Wang J., Steigmann D., Wang F.F., and Dai H.H. "On a consistent finite-strain plate theory of growth". *Journal of the Mechanics and Physics of Solids*, 111:184–214 (2018)

Wang J., Wang Q., Dai H.H., Du P., and Chen D. "Shape-programming of hyperelastic plates through differential growth: an analytical approach". *Soft matter*, 15(11):2391–2399 (2019b)

Wiggs B.R., Hrousis C.A., Drazen J.M., and Kamm R.D. "On the mechanism of mucosal folding in normal and asthmatic airways". *Journal of Applied Physiology*, 83(6):1814–1821 (1997)

Wu M. and Ben Amar M. "Growth and remodelling for profound circular wounds in skin". *Biomechanics and modeling in mechanobiology*, 14(2):357–370 (2015)

Yu X., Fu Y., and Dai H.H. "A refined dynamic finite-strain shell theory for incompressible hyperelastic materials: equations and two-dimensional shell virtual work principle". *Proceedings of the Royal Society A*, 476(2237):20200031 (2020)

A Appendix: Expression for Piola stress and unknown variables

The series expansion of deformation gradient (\mathbf{F}), elastic deformation (\mathbf{A}), inverse transpose of Growth tensor (\mathbf{G}^{-T}) and Piola Kirchhoff (\mathbf{P}) tensor are given by

$$\begin{aligned}\mathbf{F} &= \sum_{n=0}^2 \frac{Z^n}{n!} \mathbf{F}^{(n)}(\zeta) + O(Z^3), & \mathbf{A} &= \sum_{n=0}^2 \frac{Z^n}{n!} \mathbf{A}^{(n)}(\zeta) + O(Z^3), \\ \mathbf{G}^{-T} &= \sum_{n=0}^2 \frac{Z^n}{n!} \bar{\mathbf{G}}^n(\zeta) + O(Z^3), & \mathbf{P} &= \sum_{n=0}^2 \frac{Z^n}{n!} \mathbf{P}^{(n)}(\zeta) + O(Z^3).\end{aligned}\tag{A.1}$$

For an incompressible neo-Hookean material elastic strain energy function is $\phi_0(\mathbf{A}) = C_0[\text{tr}(\mathbf{A}^T \mathbf{A}) - 3]$ and the associated Piola Kirchhoff stress is given as, $\mathbf{P} = J_G [2C_0[\mathbf{A}] - p\mathbf{A}^{-T}] \mathbf{G}^{-T}$. Then, the first term in right side of the expression for \mathbf{P} in (A.1) is obtained as

$$\mathbf{P}^{(0)} = J_G \left[2C_0 \mathbf{A}^{(0)} - p \mathbf{A}^{(0)-T} \right] \bar{\mathbf{G}}^{(0)}. \tag{A.2}$$

By using bottom traction condition, $\mathbf{P}^{(0)} \mathbf{k} = \mathbf{0}$ and substituting the expression for $\mathbf{A}^{(0)}$ (see (2.6)) in (A.2) we obtain

$$2C_0 \nabla \mathbf{x}^{(0)} \bar{\mathbf{G}}^{(0)T} \hat{\mathbf{G}}^{(0)} \mathbf{k} + 2C_0 J_G |\bar{\mathbf{G}}^{(0)} \mathbf{k}|^2 \mathbf{x}^{(1)} - p^{(0)} \mathbf{F}^{(0)*} \mathbf{k} = \mathbf{0}, \tag{A.3}$$

where $J^{(0)} = J_G|_{Z=0}$, $\hat{\mathbf{G}}^{(0)} = J^{(0)} \bar{\mathbf{G}}^{(0)}$, and $\mathbf{F}^{(0)*} = \text{Cofac}(\mathbf{F}^{(0)})$. In this work, we use $\nabla \mathbf{x}^{(0)*}$ in place of $\mathbf{F}^{(0)*} \mathbf{k}$ which is given as

$$\begin{aligned}\nabla \mathbf{x}^{(0)*} &= \frac{r^{(0)}}{R} \left[\frac{\partial \theta^{(0)}}{\partial R} \frac{\partial z^{(0)}}{\partial \Theta} - \frac{\partial \theta^{(0)}}{\partial \Theta} \frac{\partial z^{(0)}}{\partial R} \right] \mathbf{e}_1 + \frac{1}{R} \left[\frac{\partial r^{(0)}}{\partial \Theta} \frac{\partial z^{(0)}}{\partial R} - \frac{\partial r^{(0)}}{\partial R} \frac{\partial z^{(0)}}{\partial \Theta} \right] \mathbf{e}_2 \\ &\quad + \frac{r^{(0)}}{R} \left[\frac{\partial r^{(0)}}{\partial R} \frac{\partial \theta^{(0)}}{\partial \Theta} - \frac{\partial \theta^{(0)}}{\partial R} \frac{\partial r^{(0)}}{\partial \Theta} \right] \mathbf{k}.\end{aligned}\tag{A.4}$$

Using incompressibility constraint $\det(\mathbf{A}) = 1$, we obtain $\det(\mathbf{F}^{(0)}) = \det(\bar{\mathbf{G}}^{(0)-T})$ which result in

$$\mathbf{x}^{(1)} \cdot \nabla \mathbf{x}^{(0)*} = \det \left(\bar{\mathbf{G}}^{(0)-T} \right), \tag{A.5}$$

where $\det(\mathbf{F}^{(0)}) = \left[r^{(1)} \mathbf{e}_1 + r^{(0)} \theta^{(1)} \mathbf{e}_2 + z^{(1)} \mathbf{e}_3 \right] \cdot \mathbf{F}^{(0)*} \mathbf{k} = \mathbf{x}^{(1)} \cdot \nabla \mathbf{x}^{(0)*}$. Using (A.3) we obtain the explicit expression for $\mathbf{x}^{(1)}$

$$\mathbf{x}^{(1)} = \frac{-2C_0 \nabla \mathbf{x}^{(0)} \bar{\mathbf{G}}^{(0)T} \hat{\mathbf{G}}^{(0)} \mathbf{k} + p^{(0)} \nabla \mathbf{x}^{(0)*}}{2C_0 J_G |\bar{\mathbf{G}}^{(0)} \mathbf{k}|^2}. \tag{A.6}$$

To obtain the explicit expression for $p^{(0)}$ we substitute (A.6) into (A.5) which yields

$$p^{(0)} = \frac{2C_0 J_G |\bar{\mathbf{G}}^{(0)} \mathbf{k}|^2}{\det \bar{\mathbf{G}}^{(0)T} |\nabla \mathbf{x}^{(0)*}|^2} + \left[2C_0 \nabla \mathbf{x}^{(0)} \bar{\mathbf{G}}^{(0)T} \hat{\mathbf{G}}^{(0)} \mathbf{k} \right] \cdot \frac{\nabla \mathbf{x}^{(0)*}}{|\nabla \mathbf{x}^{(0)*}|^2}. \tag{A.7}$$

Using Eq. (A.7), we obtain the expression for $p^{(0)}$ which is

$$p^{(0)} = \frac{2C_0\lambda^4}{|\nabla \mathbf{x}^{(0)*}|^2}, \quad (\text{A.8})$$

where $\nabla \mathbf{x}^{(0)*} = \Delta x_{11}\mathbf{e}_1 + \Delta x_{22}\mathbf{e}_2 + \Delta x_{33}\mathbf{k}$ is given by (A.4). On substituting $p^{(0)}$ in (A.6) we obtain explicit expressions for $r^{(1)}$, $\theta^{(1)}$, and $z^{(1)}$ as

$$r^{(1)} = \frac{p^{(0)}\Delta x_{11}}{2C_0\lambda^2}, \quad \theta^{(1)} = \frac{p^{(0)}\Delta x_{22}}{2C_0\lambda^2 r^{(0)}}, \quad \text{and} \quad z^{(1)} = \frac{p^{(0)}\Delta x_{33}}{2C_0\lambda^2}. \quad (\text{A.9})$$